CrossMark

Lithographed Superconducting Resonator Development for Next-Generation Frequency Multiplexing Readout of Transition-Edge Sensors

F. Faramarzi[1,2,3] · T. De Haan[2,3] · A. Kusaka[3] ·
A. Lee[2,3] · B. Neuhauser[1] · R. Plambeck[2,4] ·
C. Raum[2,4] · A. Suzuki[2,3,4] · B. Westbrook[2,4]

Abstract Ground-based cosmic microwave background (CMB) experiments are undergoing a period of exponential growth. Current experiments are observing with 1000–10,000 detectors, and the next-generation experiment (CMB stage 4) is proposing to deploy approximately 500,000 detectors. This order of magnitude increase in detector count will require a new approach for readout electronics. We have developed superconducting resonators for next-generation frequency-domain multiplexing (fMUX) readout architecture. Our goal is to reduce the physical size of resonators, such that resonators and detectors can eventually be integrated on a single wafer. To reduce the size of these resonators, we have designed spiral inductors and interdigitated capacitors that resonate around 10–100 MHz, an order of magnitude higher frequency compared to current fMUX readout systems. The higher frequency leads to a wider bandwidth and would enable higher multiplexing factor than the current ~ 50 detectors per readout channel. We will report on the simulation, fabrication method, characterization technique, and measurement of quality factor of these resonators.

Keywords Cosmic microwave background radiation · Transition-edge sensors · Frequency-domain multiplexing · Superconducting LC resonators

✉ F. Faramarzi
  ffaramar@mail.sfsu.edu

1 Department of Physics and Astronomy, San Francisco State University, San Francisco, CA 94132, USA

2 Department of Physics, University of California, Berkeley, CA 94720-7300, USA

3 Department of Physics, Lawrence Berkeley National Laboratory, Berkeley, CA 94720, USA

4 Radio Astronomy Laboratory, University of California, Berkeley, CA 94720-7300, USA

1 Introduction

Measurements of the cosmic microwave background (CMB) have revealed a wealth of information about the universe we live in. Much more information about cosmological parameters such as the equation of state of dark energy, neutrino parameters, and the energy scale of inflation is expected to be constrained by upcoming CMB experiments.

Currently, the most popular detector technology in use, in experiments such as POLARBEAR-2, Simons Array, SPT-3G, SAFARI [1–3], SPIDER, BICEP2, BICEP3, Keck Array [4], EBEX [5], SPTpol (90 GHz) [6], ABS, CLASS [7] and ACT-pol [8], consists of transition-edge sensor (TES) bolometers. Because TES bolometers are operated in a photon-noise-dominated regime, the way to increase the sensitivity of an experiment is to increase detector count.

Here, we focus on the readout of TES bolometers, using frequency-domain multiplexing (fMUX). As the detector count of experiments scales from the 10^2–10^3 regime into the 10^5–10^6 regime, fMUX technology must improve in order to keep the detector readout manageable. In this work we will present an effort to increase the available multiplexing bandwidth by designing LC resonators with higher resonance frequencies, in order to ultimately increase the multiplexing factor. The higher frequency also reduces the feature size of the multiplexing element (the LC resonators) and allows possible integration of the detectors with the resonators in future.

Current fMUX systems run with LC resonators with resonance frequencies of 5 MHz or lower. In Sect. 2, we describe the design of our superconducting inductors and capacitors with resonance frequencies up to 90 MHz. In Sect. 3, we discuss the fabrication process used for LC chips. In Sect. 4 we describe our testing methods of measuring equivalent series resistance of the resonators and will present our results.

2 Design Considerations

The primary goal is to design LC resonators with high resonance frequencies (~ 100 MHz) for which $f = 1/2\pi\sqrt{LC}$. To achieve this, one needs to design inductors and capacitors with smaller values of L and C, respectively. The capacitance of the interdigitated capacitors (IDC) can be reduced by designing capacitors with fewer fingers which in turn results in smaller sized capacitors.

One of the obstacles to design LC circuits with higher resonance frequencies is the parasitic elements in the LC components. For instance, spiral inductors have two main sources of parasitic capacitance. One is due to capacitive coupling between adjacent turns of the inductor, and the other is due to capacitive coupling to the Nb ground plane on the back of the LC chip. These extra capacitances cause the inductor to have a self-resonance frequency (SRF) of $1/2\pi\sqrt{LC_\mathrm{p}}$, where C_p is the parasitic capacitance. If this frequency is close to or lower than the resonance frequency of the LC system, then the resonators would not be able to resonate at desired frequencies. One way to reduce the capacitive coupling to the ground is to remove the Nb ground plane on the back of the chip which sits on a printed circuit board. We also lowered the inductance of the spiral inductors used in previous fMUX systems [9] from 5 to 60 μH by reducing the number of turns of each inductor and consequently reducing its size. However, if
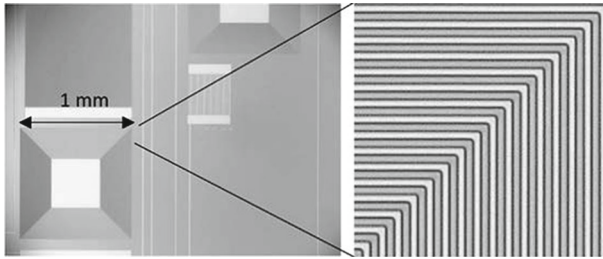
Fig. 1 Photograph of the lithographed LC resonator. The size of the inductor in this picture is 1mm × 1mm, and the linewidths are 2 μm

we adopt the 5 μH inductors we need to change the design of our current bolometers to reduce the TES resistance accordingly (∼ 10 mΩ) in order to keep the bandwidth $\Delta\omega = \frac{R}{L}$ fixed for all the LC resonators. Therefore, the requirement for ESR becomes more stringent.

Smaller LCs fulfill our second objective which is to eventually integrate the fMUX circuit into the detector wafer on the focal plane. This reduces the complexity of the large arrays and minimizes parasitic elements. We also fabricated IDCs with trace width of 2 μm to minimize the surface area of the LCs. We managed to reduce the surface area of individual inductors and capacitors to less than 1 mm^2.

Another important factor that should be taken into account is the equivalent series resistance (ESR) of the LC resonators. The LC chips do not behave like an ideal LC circuit so we expect to see some energy loss that can be modeled as a series resistance with L and C. One vital requirement for our LC design is for the ESR to be less than 10% of the bolometer resistance (R_{bolo}) which is about 1 Ω [5]. If this requirement is not met, then the power dissipated in the bolometers due to the absorption of photons becomes indistinguishable from power loss in LCs. To minimize this effect, we chose high-resistivity silicon (∼ 5000 Ω m) as our substrate with low loss tangent [10].

3 Fabrication Process

We use 150 mm silicon (Si) wafers, with resistivity of 5000 Ω m to fabricate our chips. The process involves : (1) sputtering a 300 nm layer of niobium on one side of the wafer, (2) spin coating the wafer with photoresist (PR), (3) pattering the PR using one-to-one projection lithography, (4) developing the exposed PR, (5) de-scumming of wafers with a weak oxygen plasma using a reactive ion etcher (RIE), (6) baking the remaining PR, (7) etching away the Nb with chlorine gas, and finally (8) removing the remaining PR using a PR stripper. At the end of the process, we dice the wafer.

We used Nb as our conducting trace because Nb has a high quality factor [11] and its superconducting transition temperature is 9 K. Niobium's superconducting temperature is well above the operating temperature of our detectors, and thus, the resonators are deep in transition. It is also above the temperature of liquid He which allows us to use an evaluation setup as described below. High-resistivity silicon has a relatively low loss tangent which makes it a good candidate as a dielectric.
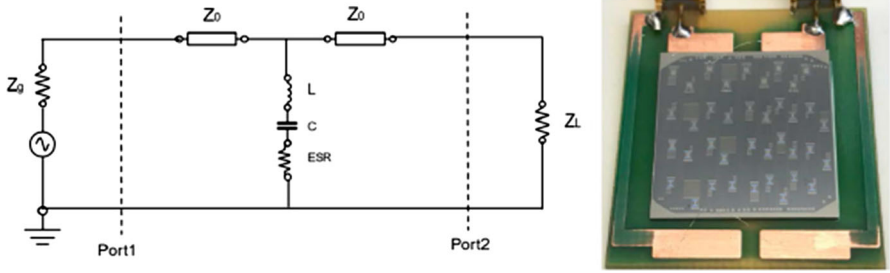
Fig. 2 *Left* is the circuit diagram of the S_{21} measurement. *Right* is the printed circuit board used to measure ESR (Color figure online)

As was mentioned in the previous section, the Nb ground plane was removed to minimize the parasitic elements. Therefore, only one side of the silicon wafer was sputtered with Nb. To reduce the size of LCs, the width of the traces was reduced to $2\,\mu$m compared to previous designs [9], as shown in Fig. 1.

4 Results

Testing was done by immersing the LC chips into liquid He-4. The boiling temperature of ^{4}He is 4 K which is five Kelvin below the superconducting transition temperature of Nb. The LC chip was mounted and wirebonded to a printed circuit board (PCB) using aluminum (Al) bond wires. To measure the ESR of LC resonators at frequencies close to 100 MHz where parasitics are more significant, we need a method that is robust against those effects. A two-port shunt measurement technique is the RF equivalent of the four-point measurement, and it is sensitive to very low impedances [12]. If we calculate the impedance of the LRC circuit in Fig. 2 using the S_{21} parameter, then the impedance is related to the S_{21} by Eq. (1).

$$Z_{\mathrm{LRC}} = 25\,\frac{S_{21}}{1 - S_{21}}\,\Omega \tag{1}$$

At the resonance frequency, the reactive part of the impedance is zero. Therefore, Z_{LRC} gives us the ESR of the resonators. It is important to mention that the impedance calculated with this method is the impedance of LRC and other possible parasitic elements that are either in series or parallel with the LC chip. To minimize the parasitic effects, two bond wires were used to connect port one and port two of the PCB to one leg of the LC chip and two other bond wires to connect the other leg of the LC chip to grounds of port one and two. This way the grounds of both ports are connected at the LC which minimizes the possible parasitic elements in series with the chip. Finally, both ports of the PCB are connected to a vector network analyzer (VNA) through an SMA cable.

The *left* plot of Fig. 3 shows the S_{21} versus frequency measurement of an LC resonator with resonance frequency of 42 MHz, The measured ESR from this plot is $50 \pm 10\,\mathrm{m}\Omega$. The *right* plot shows the same measurement for an LC with resonance
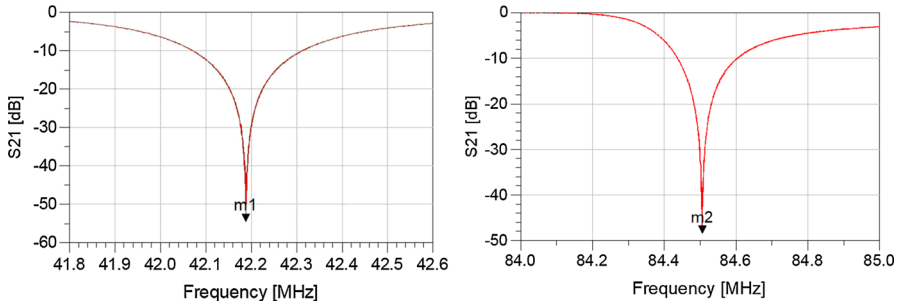
Fig. 3 *Left* is the S_{21} measurement of a 42 MHz LC resonator. *Right* is the S_{21} measurement of a 84 MHz LC resonator. Both of these measurement were done using an input power of -65 dBm (Color figure online)
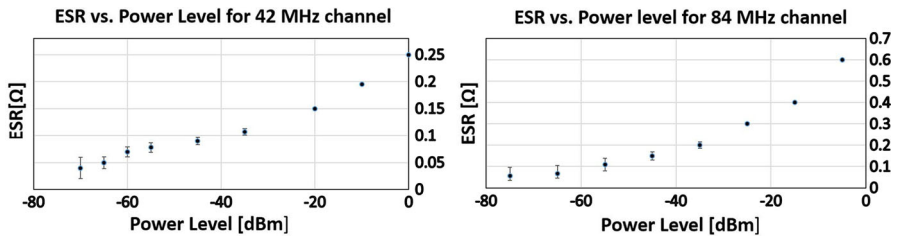
Fig. 4 *Left* plot of equivalent series resistance versus input power for an LC with resonance frequency of 42 MHz. *Right* same measurement for an LC with resonance frequency of 84 MHz (Color figure online)

frequency of 82 MHz, and the measured ESR is 90 $\pm$10 mΩ. The inductance of the tested resonators is 5 μH, and both are compact-LC circuits with trace width of 2 μm. The input power of the VNA for these measurements was set to -65 dBm using a series of -10 dB attenuators. The ESR of each resonator was measured with different input powers, and as we can see in Fig. 4 an excitation-dependent loss is observed in the resonators. We speculate that this effect could arise due to one of the following reasons: exceeding the critical current density of Nb films at around -40 dBm [13] or very high magnetic field densities around the sharp corners of the square spiral inductor [14].

In summary, we designed LC resonators with resonance frequencies up to 84 MHz by increasing the self-resonance frequency of our planar inductors. The LC resonators are also small in size and therefore capable of being integrated on the focal plane of the telescope. Our results show that at power levels used in CMB experiments (~ -110 dBm) the ESR of the LC resonators decreases to ~ 50 mΩ. In order to use the 5 μH inductors we need to further investigate means to reduce the ESR of our resonators to ~ 10 mΩ. However, since the ESR is frequency-dependent [10], we can implement the present design inductors for frequencies up to 20 MHz.

References

1. A. Suzuki, P. Ade, Y. Akiba, C. Aleman, K. Arnold, C. Baccigalupi, B. Barch, D. Barron, A. Bender, D. Boettger, J. Borri, S. Chapman, Y. Chinone, A. Cukierman, M. Dobbs, A. Ducout, R. Dunner, T. Elleflot, J. Errard, G. Fabbian, S. Feeney, C. Feng, T. Fujino, G. Fuller, A. Gilbert, N. Goeckner-Wald, J. Groh, T. De Haan, G. Hall, N. Halverson, T. Hamada, M. Hasegawa, K. Hattori, M. Hazumi, C. Hill, W. Holzapfe, Y. Hori, L. Howe, Y. Inoue, F. Irie, G. Jaehnig, A. Jaffe, O. Jeong, N. Katayama, J. Kaufman, K. Kazemzadeh, B. Keating, Z. Kermish, R. Keskitalo, T. Kisner, A. Kusaka, M. Le Jeune, A. Lee, D. Leon, E. Linder, L. Lowry, F. Matsuda, T. Matsumura, N. Miller, K. Mizukami, J. Montgomery, M. Navaroli, H. Nishino, J. Peloton, D. Poletti, G. Puglisi, G. Rebeiz, C. Raum, C. Reichardt, P. Richards, C. Ross, K. Rotermund, Y. Segawa, B. Sherwin, I. Shirley, P. Siritanasak, N. Stebor, R. Stompor, J. Suzuki, O. Tajima, S. Takada, S. Takakura, S. Takatori, A. Tikhomirov, T. Tomaru, B. Westbrook, N. Whitehorn, T. Yamashita, A. Zahn, O. Zahn, J. Low Temp. Phys. **184**, 805 (2016). https://doi.org/10.1007/s10909-015-1425-4

2. B.A. Benson, P.A.R. Ade, Z. Ahmed, S.W. Allen, K. Arnold, J.E. Austermann, A.N. Bender, L.E. Bleem, J.E. Carlstrom, C.L. Chang, H.M. Cho, J.F. Cliche, T.M. Crawford, A. Cukierman, T. de Haan, M.A. Dobbs, D. Dutcher, W. Everett, A. Gilbert, N.W. Halverson, D. Hanson, N.L. Harrington, K. Hattori, J.W. Henning, G.C. Hilton, G.P. Holder, W.L. Holzapfel, K.D. Irwin, R. Keisler, L. Knox, D. Kubik, C.L. Kuo, A.T. Lee, E.M. Leitch, D. Li, M. McDonald, S.S. Meyer, J. Montgomery, M. Myers, T. Natoli, H. Nguyen, V. Novosad, S. Padin, Z. Pan, J. Pearson, C. Reichardt, J.E. Ruhl, B.R. Saliwanchik, G. Simard, G. Smecher, J.T. Sayre, E. Shirokoff, A.A. Stark, K. Story, A. Suzuki, K.L. Thompson, C. Tucker, K. Vanderlinde, J.D. Vieira, A. Vikhlinin, G. Wang, V. Yefremenko, K.W. Yoon (2014). Proc. SPIE 9153, Millimeter, Submillimeter, and Far-Infrared Detectors and Instrumentation for Astronomy VII, https://doi.org/10.1117/12.2057305

3. M.P. Bruijn, L. Gottardi, R.H. den Hartog, H.F.C. Hoevers, M. Kiviranta, P.A.J. de Korte, J. van der Kuur, J. Low Temp. Phys. **167**, 695 (2012). https://doi.org/10.1007/s10909-011-0422-5

4. C.L. Kuo, J.J. Bock, J.A. Bonetti, J. Brevik, G. Chattopadhyay, P.K. Day, S. Golwala, M. Kenyon, A.E. Lange, H.G. LeDuc, H. Nguyen, R.W. Ogburn, A. Orlando, A. Transgrud, A. Turner, G. Wang, J. Zmuidzinas, Proc. SPIE 7020, Millimeter and Submillimeter Detectors and Instrumentation for Astronomy IV (2008). https://doi.org/10.1117/12.788588

5. A.M. Aboobaker, P. Ade, D. Araujo, F. Aubin, C. Baccigalupi, B. C., D. Chapman, J. Didier, M. Dobbs, C. Geach, W. Grainger, S. Hanany, K. Helson, S. Hillbrand, J. Hubmayr, A. Jaffe, B. Johnson, T. Jones, J. Klein, A. Korotkov, A. Lee, L. Levinson, M. Limon, K. MacDermid, T. Matsumura, A.D. Miller, M. Milligan, K. Raach, B. Reichborn-Kjennerud, I. Sagiv, G. Savini, L. Spencer, C. Tucker, G. Tucker, B. Westbrook, K. Young, K. Zilic, The EBEX Balloon Borne Experiment-Optics, Receiver, and Polarimetry, arXiv:1703.03847 (2017)

6. J.T. Sayre, P. Ade, K.A. Aird, J.E. Austermann, J.A. Beall, D. Becker, B.A. Benson, L.E. Bleem, J. Britton, J.E. Carlstrom, C.L. Chang, H.-M. Cho, T.M. Crawford, A.T. Crites, A. Datesman, T. de Haan, M.A. Dobbs, W. Everett, A. Ewall-Wice, E.M. George, N.W. Halverson, N. Harrington, J.W. Henning, G.C. Hilton, W.L. Holzapfel, J. Hubmayr, K.D. Irwin, M. Karfunkle, R. Keisler, J. Kennedy, A.T. Lee, E. Leitch, D. Li, M. Lueker, D.P. Marrone, J.J. McMahon, J. Mehl, S.S. Meyer, J. Montgomery, T.E. Montroy, J. Nagy, T. Natoli, J.P. Nibarger, M.D. Niemack, V. Novosad, S. Padin, C. Pryke, C.L. Reichardt, J.E. Ruhl, B.R. Saliwanchik, K.K. Schaffer, E. Shirokoff, K. Story, C. Tucker, K. Vanderlinde, J.D. Vieira, G. Wang, R. Williamson, V. Yefremenko, K.W. Yoon, E. Young, Millimeter, Submillimeter, and Far-Infrared Detectors and Instrumentation for Astronomy VI **8452**, 845239 (2012). https://doi.org/10.1117/12.927035

7. K.L. Denis, A. Ali, J. Appel, C.L. Bennett, M.P. Chang, D.T. Chuss, F.A. Colazo, N. Costen, T. Essinger-Hileman, R. Hu, T. Marriage, K. Rostem, K. U-Yen, E.J. Wollack, J. Wollack, J. Low Temp. Phys. **184**, 668 (2016). https://doi.org/10.1007/s10909-015-1366-y

8. R.J. Thornton, P.A.R. Ade, S. Aiola, F.E. Angile, M. Amiri, J.A. Beall, D.T. Becker, H. Cho, S.K. Choi, P. Corlies, K.P. Coughlin, R. Datta, M.J. Devlin, S.R. Dicker, R. Dunner, J.W. Fowler, A.E. Fox, P.A. Gallardo, J. Gao, E. Grace, M. Halpern, M. Hasselfield, S.W. Henderson, G.C. Hilton, A.D. Hincks, S.P. Ho, J. Hubmayr, K.D. Irwin, J. Klein, B. Koopman, D. Li, T. Louis, M. Lungu, L. Maurin, J. McMahon, C.D. Munson, S. Naess, F. Nati, L. Newburgh, J. Nibarger, M.D. Niemack, P. Niraula, M.R. Nolta, L.A. Page, C.G. Pappas, A. Schillaci, B.L. Schmitt, N. Sehgal, J.L. Sievers, S.M. Simon, S.T. Staggs, C. Tucker, M. Uehara, J. van Lanen, J.T. Ward, E.J. Wollack, ApJ **227**, 21 (2016). https://doi.org/10.3847/1538-4365/227/2/21

9. K. Rotermund, B. Barch, S. Chapman, K. Hattori, A. Lee, N. Palaio, I. Shirley, A. Suzuki, C. Tran, J. Low Temp. Phys. **184**, 486 (2016). https://doi.org/10.1007/s10909-016-1554-4
10. K. Hattori et al., Nucl. Instr. Methods Phys. Res. **732**, 299 (2013). https://doi.org/10.1016/j.nima.2013.07.052
11. J.P. Turneaure, I. Weissman, J. Appl. phys. **39**, 4417 (1968)
12. Ultra-Low Impedance Measurements Using 2-Port Measurements, Agilent Technologies application note, 5989-5935EN, 13 (2007)
13. W.R. Hudson, R.J. Jirberg, NASA Technical note, NASA TN D-6380 (1971)
14. R. Brambilla, F. Grilli, L. Martini, Supercond. Sci. Technol. **20**, 16 (2007)